

Journal of Materials Chemistry A

Accepted Manuscript



This is an *Accepted Manuscript*, which has been through the Royal Society of Chemistry peer review process and has been accepted for publication.

Accepted Manuscripts are published online shortly after acceptance, before technical editing, formatting and proof reading. Using this free service, authors can make their results available to the community, in citable form, before we publish the edited article. We will replace this *Accepted Manuscript* with the edited and formatted *Advance Article* as soon as it is available.

You can find more information about *Accepted Manuscripts* in the [Information for Authors](#).

Please note that technical editing may introduce minor changes to the text and/or graphics, which may alter content. The journal's standard [Terms & Conditions](#) and the [Ethical guidelines](#) still apply. In no event shall the Royal Society of Chemistry be held responsible for any errors or omissions in this *Accepted Manuscript* or any consequences arising from the use of any information it contains.



www.rsc.org/materialsA

ARTICLE

Multifunctional fullerene interlayer in colloidal quantum dot-based hybrid solar cells

Cite this: DOI: 10.1039/x0xx00000x

Minwoo Nam,^a Joongpill Park,^b Keekeun Lee,^c Sang-Wook Kim,^b Hyunduk Ko,^a Il Ki Han^{*a} and Doo-Hyun Ko^{*a,d}

Received 00th January 2015,
Accepted 00th January 2015

DOI: 10.1039/x0xx00000x

www.rsc.org/

Chemically modifying the surfaces of colloidal quantum dots (QDs) offers an effective approach to improving their photovoltaic performances. Ligand exchange processes, however, tend to cause nanoscale cracks throughout the QD-based films, which increases the leakage current and magnitude of recombination losses. Here, we have developed a multifunctional [6,6]-phenyl C₆₁ butyric acid methyl ester (PC₆₀BM) cathode interlayer for use in polymer-QD hybrid bulk heterojunction (BHJ) solar cells. The PC₆₀BM layer deposited onto the hybrid BHJ film via solution uniformly covered the nanocracks produced by QD surface ligand exchange with thiol and facilitated electron transport to the cathode. The PC₆₀BM layer also improved photon harvesting at short wavelengths and formed an efficient vertical donor:acceptor/acceptor' (D:A/A') junction in the interfacial areas between the hybrid blend and the PC₆₀BM. The efficient vertical junction increased the probability of ultrafast exciton dissociation, provided pathways for effective transport and extraction of photo-generated electrons, and blocked holes to reduce recombination losses. These combined advantages significantly enhanced the overall efficiency of the hybrid solar cells over the current state-of-the-art efficiency.

Introduction

Organic–inorganic hybrid solar cells (HSCs), which consist of bulk heterojunctions (BHJs) composed of conjugated polymers as electron donors and colloidal quantum dots (QDs) as electron acceptors, combine the advantages of the two material classes.¹ Polymers have film-forming property and provide a high absorption coefficient, whereas QDs have size-tunable band gaps, offer broad light absorption, and can generate multiple excitons from a single photon.^{2–7} The efficiency of HSCs has been significantly enhanced through advances in synthesis, processing, and surface chemistry of QDs over the last few years. For instance, post-deposition exchange of long-chain organic ligands (e.g., oleic acid) that wrap around the as-synthesized QD surfaces with short functional molecules (e.g., thiol and amine groups) can improve the interfacial contacts between the polymer and QDs, improve the QD-based film conductivity, and increase QD surface passivation, leading to enhanced charge transfer and reduced recombination sites.^{8–12} The ligand treatment technique addresses the main factor that limits HSCs: the lack of control over the interface between the heterogeneous organic and inorganic materials. In previous reports, we successfully described broadband energy-harvesting HSCs with power conversion efficiencies (PCEs) exceeding 3% by using engineered donor–acceptor (D–A) interfaces in which the lead sulfide (PbS) QD surfaces were modified with thiol ligands.^{13,14} However, these benefits come at a cost in that the post-deposition ligand treatment causes nanoscale cracks and pinholes on the blend film surface due to changes in the free volume and polarity during the ligand exchange process.^{15–17} The cracks increase the leakage current, introduce serious recombination losses, and are the main cause of the relatively low fill factors (FFs) of

HSCs, typically 40–50% or lower,^{9–11,16} compared to the FFs obtained in organic solar cells (OSCs), which can exceed 70%.^{18,19}

This study describes and implements a new design platform for developing high-efficiency HSCs employing a fullerene interlayer between the PbS QD-based hybrid blend and the top electrode. We concentrated on the attributes of [6,6]-phenyl C₆₁ butyric acid methyl ester (PC₆₀BM) as a cathode interlayer material, which provides a high electron mobility, high electron affinity, deep ionization potential, small particle size, and film uniformity. In the device, the poly((4,8-bis(octyloxy)benzo(1,2-*b*:4,5-*b'*)dithiophene-2,6-diyl)(2-((dodecyloxy)carbonyl)thieno(3,4-*b*)thiophenediyl)) (PTB1):PbS QD blend and upper PC₆₀BM interlayer formed vertical donor:acceptor/acceptor' (D:A/A') junctions, in which electrons segregated in the hybrid blend in contact with PC₆₀BM could diffuse through the PC₆₀BM layer to the Al electrodes by virtue of favorable junction formation. The PbS QDs in the hybrid blend received photo-generated electrons from PTB1 as an electron acceptor²⁰ but also simultaneously donated electrons to the upper PC₆₀BM layer as an electron donor, enabled by the ambipolar transport properties of PbS QDs. Multiple investigations revealed that an optimally thin PC₆₀BM layer improved exciton generation, facilitated exciton dissociation into free charge carriers, and provided pathways for effective electron extraction. These benefits led us to attain an overall efficiency approaching 4.53%, which is the highest value yet reported for PbS-based HSCs to the extent of our knowledge.

Results and discussion

Fig. 1a shows the ultraviolet (UV)–vis–near infrared (NIR) absorption spectra of pure films composed of PTB1 or PbS QDs (the chemical structure of PTB1 and the type-II heterojunction at the

hybrid interface are depicted as well). The absorption of the PbS QDs extended from the UV to the NIR regions, but the absorption properties in the visible region were relatively low due to the sparse density of states between the 1st and 2nd excitons. The strong absorption properties of PTB1 in the visible range between 500 nm and 800 nm could complement the low absorption of the QDs in that region, thereby allowing broadband photon harvesting in the PTB1:PbS hybrid blends. The absorption spectra of the PTB1:PbS hybrid blends ranged broadly from the UV to the NIR regions with no significant drop in the absorption profile (Fig. 1b). The absorption spectrum reflected the concentration of PbS QDs present in the polymer matrix and approached the QD absorption spectrum as the PTB1:PbS QD weight ratio increased from 1:2 to 1:19.

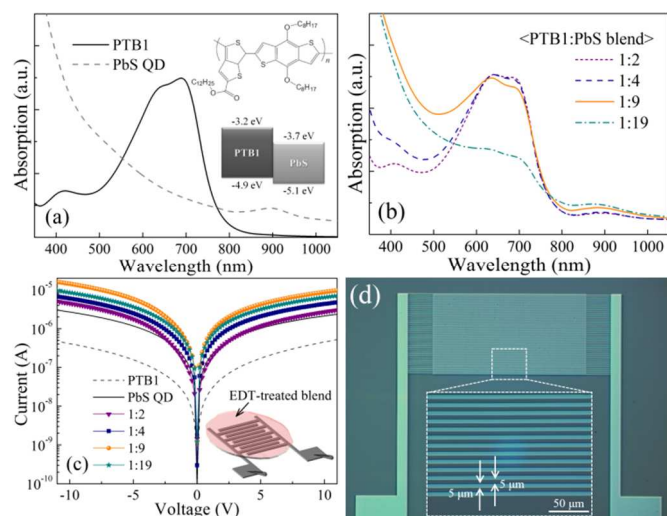


Fig. 1. Absorption spectra of (a) the pure PTB1 and PbS QD films, and (b) PTB1:PbS hybrid blends as a function of the polymer-to-QD ratio. (c) $I-V$ characteristics of the hybrid blends, measured at interdigitated finger-like electrodes under UV illumination, and (d) optical microscopy images of the interdigitated electrodes deposited on a glass substrate.

Exciton dissociation at the interface between PTB1 and the thiol-treated PbS QDs and hole transfer from the QDs to the polymer were investigated via facile photocurrent measurements collected from the hybrid blends, because thiol-treated PbS QDs are primarily considered as p-type materials. The hole transfer dynamics were examined by illuminating with 365 nm UV light, which is absorbed by the PbS QDs to generate excitons but is not absorbed well by the PTB1, whereas the visible light excites both the polymer and QDs, as shown in Fig. 1a and b. Fig. 1c shows the current-to-voltage ($I-V$) characteristics of the films under UV illumination. A 100 μL blend solution in chloroform was spin-coated onto a set of 5 μm wide interdigitated finger-like Au electrodes separated by 5 μm spacings on a standard glass substrate. The thicknesses of the blend films prepared with different D-A ratios were fixed similarly at a given value. Fig. 1d shows optical microscopy images of interdigitated Au electrodes fabricated via a lift-off process (details are provided in Experimental Section). The photocurrent in the hybrid blends was consistently higher than the photocurrents measured in pure films composed of PTB1 or PbS QDs; for instance, the 1:9 blend biased at 10 V under illumination produced a photocurrent of 8.76 μA , whereas the device composed of a pure PTB1 film and a pure PbS QD film showed significantly lower photocurrents of 0.45 μA and 2.18 μA , respectively. These results suggested that efficient exciton dissociation and photo-excited hole transfer from the PbS QDs to the PTB1 took place prior to recombination via the formation of D-A

heterojunctions between the polymer and the PbS QDs. By contrast, poor light absorption in the UV region and the absence of a charge transfer phase in the pure films limited the current generation. We also found that the $I-V$ characteristics depended on the blending ratio between the D-A components, and devices based on a PTB1-to-PbS ratio of 1:9 showed the highest photocurrent among devices. An optimal density of the QDs in the polymer matrix and efficient interactive networks between the two components may together improve exciton dissociation and charge transfer at the heterojunction interfaces, which are prerequisites for efficient photovoltaics. The experimental results suggested that PbS QDs could provide ambipolar transport, which permits photo-excited hole transfer toward the polymer through an efficient type-II heterojunction system (as a n-type acceptor), but also photo-excited electron transfer toward an electron acceptor, provided that an extra electron acceptor with strong n-type character is added (e.g., PC₆₀BM) and then couples to the thiol-treated PbS QDs in the polymer-QD-fullerene ternary heterojunction system (as a p-type donor). The ambipolar transport could be enabled by a relatively weak p-type character of the thiol-treated PbS QDs with a low doping density of around 10^{14} cm^{-3} .²¹

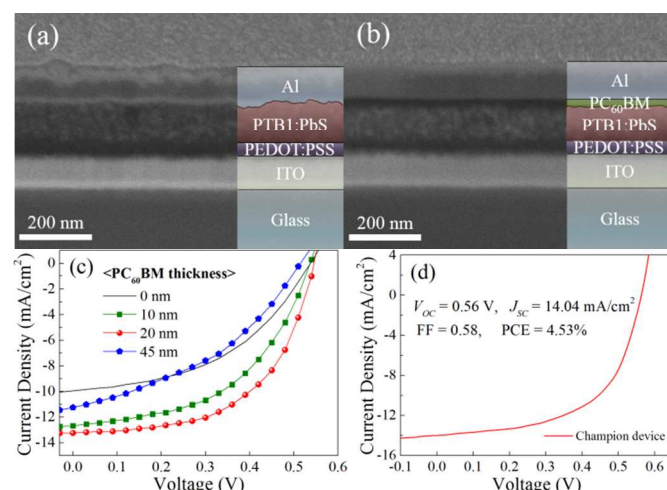


Fig. 2. Cross-sectional SEM images of the HSCs prepared (a) without or (b) with a 20 nm thick PC₆₀BM interlayer. $J-V$ characteristics of (c) the HSCs developed with different PC₆₀BM thicknesses under AM 1.5G illumination, and (d) a representative device prepared with a 20 nm thick PC₆₀BM layer, selected from among more than twenty identical cells.

HSCs were fabricated using a nanocomposite composed of PTB1 and PbS QDs in a blending ratio of 1:9. Fig. 2a and b, respectively, show cross-sectional scanning electron microscopy (SEM) images of two devices prepared without or with a thin PC₆₀BM interlayer between the hybrid blend and the top Al electrode. Sequential layers of indium tin oxide (ITO)/poly(3,4-ethylenedioxythiophene)-poly(styrenesulfonate) (PEDOT:PSS)/hybrid blend/PC₆₀BM/Al may be easily distinguished in the image. The thicknesses of the PC₆₀BM interlayers were 9–12 nm (*ca.* 10 nm), 17–21 nm (*ca.* 20 nm), and 45–47 nm (*ca.* 45 nm), and could be controlled by varying the solution concentration and spin-coating speed. Each series of devices were fabricated and tested under the identical conditions for strict comparison between them, and some unintentional variables in the process were set to be minimized.

Fig. 2c shows the current density-to-voltage ($J-V$) characteristics of the HSCs as a function of PC₆₀BM layer thickness under Air Mass 1.5 Global (AM 1.5G) illumination (100 mW/cm^2), and Table I summarizes the photovoltaic performance parameters obtained.

The device prepared without a PC₆₀BM layer exhibited an open-circuit voltage (V_{OC}) of 0.54 V, a short-circuit current density (J_{SC}) of 9.45 mA/cm², a FF of 0.46, and a PCE of 2.34%. The introduction of a 10 nm thick PC₆₀BM cathode interlayer into the HSC increased the PCE to 3.39% due to increases in both J_{SC} to 12.68 mA/cm² and FF to 0.5. A PCE approaching 3.98% was achieved by incorporating the 20 nm thick PC₆₀BM layer, yielding a V_{OC} , J_{SC} , and FF of 0.55 V, 13.24 mA/cm², and 0.55, respectively. The best device obtained among more than 20 cells fabricated under identical conditions provided a V_{OC} of 0.56 V, J_{SC} of 14.04 mA/cm², FF of 0.58, and PCE of 4.53% (Fig. 2d). To the best of our knowledge, the overall efficiency obtained in this study is the highest value yet reported using PbS-based hybrid BHJ solar cells^{13,16,22,23} (although the PCE still lags behind high PCEs in all-inorganic QD solar cells approaching 8% or more).^{24,25} Further increases in the PC₆₀BM thickness to 45 nm significantly decreased the PCE to 2.3%, similar to the values of the reference HSC without a PC₆₀BM layer. The only difference between the devices was the thickness of the PC₆₀BM interlayer, indicating that the PC₆₀BM interlayer significantly contributed to the photovoltaic performances (optical, electronic, and/or morphological properties) of the HSCs.

Table 1. The photovoltaic parameters, representing the average of the measurements collected from at least fifteen cells.

PC ₆₀ BM thickness	V_{OC} (V)	J_{SC} (mA/cm ²)	FF	PCE (%)
0 nm	0.54	9.45	0.46	2.34
10 nm	0.54	12.68	0.50	3.39
20 nm	0.55	13.24	0.55	3.98
20 nm (Best)	0.56	14.04	0.58	4.53
45 nm	0.51	11.25	0.40	2.30

First, we examined the optical properties of PC₆₀BM that can generate excitons through photon absorption at short wavelengths of the solar spectrum. The optical effects were explored by measuring the absorption spectra of the PTB1:PbS blend films with or without a 20 nm thick PC₆₀BM layer, as shown in Fig. 3a. The absorption in the UV region between 250 and 450 nm was higher for the PC₆₀BM-inserted sample. This result indicated that the upper PC₆₀BM layer absorbed photons in the UV range that were not fully harvested by the hybrid blend. However, the absorption profile of the PC₆₀BM overlapped with the PbS QDs and the absorption enhancement was confined to the UV area in which the spectral power of the sun is relatively weak (as illustrated in the graph). It was therefore difficult to determine that PC₆₀BM significantly improved the efficiencies of the HSCs by increasing light absorption. We next explored the other effects of PC₆₀BM that improved the overall efficiency of the HSCs.

Photoluminescence (PL) quenching measurements were performed to examine the exciton transfer dynamics in the device, because PL quenching is a simple but highly useful tool for understanding charge separation and transfer dynamics between the heterojunction components.²⁶⁻³¹ Fig. 3b shows the normalized PL intensity spectra of three films composed of PbS QDs, a PTB1:PbS QD blend, and a PTB1:PbS QD/PC₆₀BM blend. It should be noted that the PL signal for PTB1 and PC₆₀BM materials was not observed above 900 nm, and the observed PL signal fully arose from the PbS QDs. The PL of the PTB1:PbS blend was significantly quenched relative to the strong PL intensity measured in the pure PbS QD film, suggesting that ultrafast photo-induced charge transfer occurred between the two components. PL quenching is a prerequisite for efficient HSC operation.³² Because no PL signal was obtained from the PTB1 in the NIR region, the PL quenching was fully attributed to the dissociation of excitons generated in the QDs and the subsequent hole transfer from the QDs to the polymer. These effects also

indicated the formation of a charge-separating type-II band offset at the PTB1:PbS interfaces. The PL signal was nearly completely quenched upon incorporation of a PC₆₀BM layer into the hybrid blend. Complete PL quenching may have resulted from the additional migration of electrons from the PbS QDs to the PC₆₀BM, whereas holes transferred from the PbS QDs to the PTB1. The PC₆₀BM layer facilitated ambipolar charge transport within the PbS QDs, as expected based on the I - V results collected under UV illumination (see Fig. 1c). Hole transfer to the polymer determined the equilibrium population in the QDs after electron transfer to the PC₆₀BM, thereby allowing for re-excitation and new charge transfer.³³ The device, thus, could trap fewer photo-generated charges due to the presence of the separate PC₆₀BM layer.

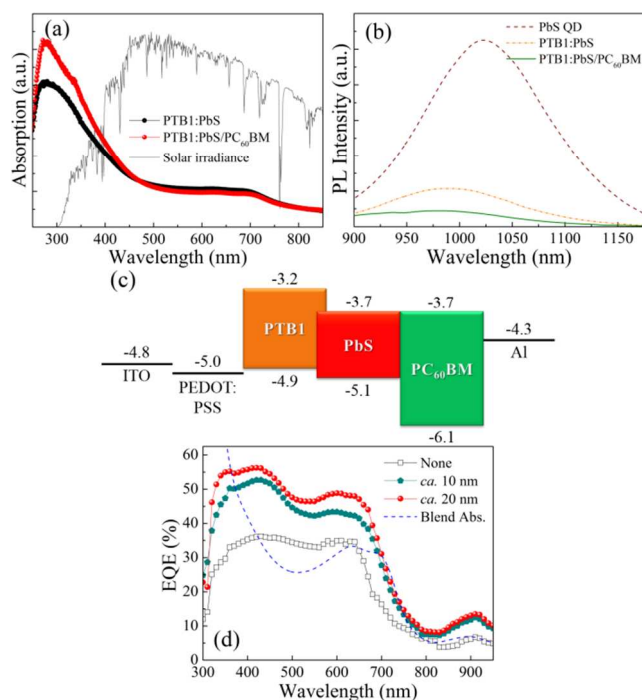


Fig. 3. (a) Absorption spectra of the PTB1:PbS blends prepared without or with a 20 nm thick PC₆₀BM layer. (b) Normalized PL intensity spectra of the pure PbS QD, PTB1:PbS blend, and PTB1:PbS/PC₆₀BM films. (c) Energy band diagram of the overall HSC prepared with a thin PC₆₀BM cathode interlayer. (d) EQE spectra as a function of PC₆₀BM layer thickness.

The LUMO level of the PC₆₀BM is similar to the conduction band (CB) of the PbS QDs (3.5 nm in diameter),³⁴ whereas its HOMO level is as deep as 6.1 eV (see Fig. 3c). PC₆₀BM in the HSC can effectively function as an intermediate to transport electrons toward the top Al electrode, and its deep HOMO level blocks holes and reduces carrier recombination loss. The PC₆₀BM interlayer also provides an extra interface for ultrafast exciton dissociation via the formation of vertical hybrid interfaces with the polymer:QD composite. PC₆₀BM is a semiconductor with strong n-type character, whereas PTB1 and PbS are typically considered as p-type semiconductors (even if they display ambipolar transport properties).^{35,36} Our device appeared to have a 'self-assembled D:A/A' structure',¹⁷ in which each solar cell, based on a purely organic PTB1:PC₆₀BM BHJ film³⁷ or a hybrid PbS QD:PC₆₀BM BHJ film,³⁸ operated well individually: in particular, PTB1 is one of the highly efficient donor polymers in OSCs with a high PCE of around 5%. The PC₆₀BM interlayer appeared to increase the dissociation of photo-excited excitons, their transport, and their extraction toward the electrode. These electronic advantages are

strongly associated with an increase in J_{SC} in PC₆₀BM-inserted devices.

To underpin the assumption, external quantum efficiency (EQE) spectra of the devices were compared, because EQE is determined from the products in consecutive steps of photon absorption, photo-excited carrier diffusion, exciton dissociation, charge transport, and charge collection at the electrodes. Fig. 3d compares the EQE spectra of the HSCs with or without a thin PC₆₀BM interlayer: the J_{SC} values calculated from the EQE spectra agreed well with the J_{SC} values extracted from the J - V curves. A significant increase in the EQE of the PC₆₀BM-inserted HSCs over the entire spectral range indicated enhanced charge generation kinetics due to the presence of the PC₆₀BM layer. The EQE spectra of the PC₆₀BM-inserted HSCs exhibited two broad peaks at 330 – 470 nm and 570 – 650 nm, which corresponded to the active absorption ranges of the PbS QDs and PTB1, respectively. These results indicated enhanced charge generation dynamics in the fine D:A/A' structure, such that both PTB1 and PbS QDs displayed a higher probability of exciton dissociation and transfer in their respective junctions formed by a strong n-type PC₆₀BM. The EQE spectrum indeed reflected a superposition of the respective EQE spectra of the binary devices based on PbS:PC₆₀BM³⁹ and PTB1:PC₆₀BM.³⁷ We believe that the inserted PC₆₀BM layer improved the photocurrent in the overall devices by enhancing the exciton dissociation probability and providing effective pathways for efficient electron transport and extraction. To examine how much of the increase in the J_{SC} was from PTB1-PC₆₀BM interaction and from PbS QD-PC₆₀BM interaction, we extracted the J_{SC} of the devices in three respective wavelength ranges of 300 – 500 nm, 510 – 800 nm, and 810 – 1100 nm. The J_{SC} can be theoretically calculated by integrating the product of the incident photon flux density $F(\lambda)$ and EQE(λ) of the device over the wavelength (λ) of the incident light,

$$J_{SC} = \int qF(\lambda)(1 - r(\lambda))EQE(\lambda)d\lambda$$

where q is the electron charge and $r(\lambda)$ is the incident light loss in light absorption.⁴⁰ Based on our calculation using the experimentally obtained EQE spectra, the J_{SC} was increased from 5.50 to 7.93 mA/cm² in the wavelength of 510 – 800 nm (main absorption area of the PTB1), corresponding to the enhancement ratio of 44.18%, when compared to two HSCs with and without the 20 nm thick PC₆₀BM layer. The J_{SC} was also 46.24% (from 2.66 to 3.89 mA/cm²) and 85.25% (from 0.61 to 1.13 mA/cm²) increased at wavelength regions below 500 nm and beyond 800 nm (where PTB1 hardly absorbs photons), respectively. These indicated that efficient interactions between PTB1/PC₆₀BM as well as QD/PC₆₀BM contributed to the photovoltaic performance enhancement in the PC₆₀BM-inserted HSCs. However, the J_{SC} in the wavelength region of 510 – 800 nm holds more than half of the total J_{SC} in the devices because of the strong solar intensity in that wavelength region. It signifies that the effective coupling between PTB1/PC₆₀BM and resultant enhancement in the EQE in the visible wavelength of 510 – 800 nm are an important source of the J_{SC} increase in the PC₆₀BM-inserted HSCs.

In an OSC, an n-type interlayer on top of a polymer:fullerene film can improve photo-excited electron extraction to the top electrode but also offer enhanced electrical contact between the photoactive layer and the cathode.⁴¹ Microscopy techniques were next used to explore whether the PC₆₀BM layer offers such morphological effect on the HSCs. Fig. 4a and b show SEM and atomic force microscopy (AFM) images of the PTB1:PbS QD blend before and after applying the PC₆₀BM coating. Nanoscale cracks and pinholes were observed on the surface of the ligand-treated hybrid blend because the surface properties changed after the free volume and polarity changed during

the post-deposition ligand treatment: the short ligands (here, 1,2-ethanedithiol, EDT) could not completely fill the space taken up by the initial long ligands (here, oleic acid).¹⁷ By contrast, the uniformity of the surface was improved after the deposition of a thin PC₆₀BM layer, which formed a conformal coating on the hybrid blend layer and completely filled the nanocracks (Fig. 4b). It has been previously reported that a uniform metal oxide nanoparticle (NP) interlayer (e.g., TiO₂) deposited on a ligand-treated hybrid blend layer can improve electrical contact between the photoactive film and the cathode by reducing the contact resistance.¹⁶ However, the extremely small PC₆₀BM particle size, which is smaller than the size of the typical TiO₂ NPs,⁴² permits more efficient diffusion of PC₆₀BM into nanoscale cracks and formation of better contact between the photoactive layer and the top electrode, compared to the cases of metal oxide NPs. Interestingly, this effect was observed in the cross-sectional SEM images shown in Fig. 2a and b, in which the photoactive film–metal interface flattened in the presence of the thin PC₆₀BM layer. The interfacial contacts were highly rough in the absence of the interlayer. The thin PC₆₀BM layer provided a uniform interlayer that improved contact at the semiconductor–metal interface, suppressed carrier recombination, and facilitated carrier extraction. These results fully interpret the simultaneous enhancement in the J_{SC} and FF in HSCs developed with an optimally thick PC₆₀BM layer. It should be pointed out that the optimized PC₆₀BM-inserted HSCs provided a relatively high FF of 0.58, although a thin electron-collecting metal layer such as LiF was not used.⁴³

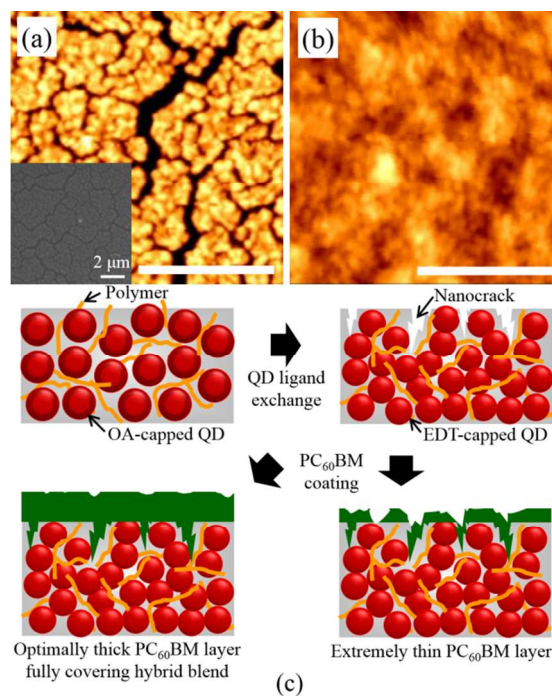


Fig. 4. SEM image and AFM surface topographies of the ligand-treated PTB1:PbS blend films (a) before and (b) after applying a PC₆₀BM coating (scale bars indicate 500 nm). (c) Cross-sectional schematic diagram of the morphological changes displayed by the photoactive blend film as a function of the surface ligand treatment and thickness of the PC₆₀BM layer.

Fig. 4c schematically illustrates the morphological structures of the photoactive films prepared with different PC₆₀BM layer thicknesses. The film morphology significantly influenced the

overall efficiency of the HSCs. After exchanging the initial oleic acid ligands on the QD surface with short EDT molecules, the distance between the QDs and the polymer (as well as between neighboring QDs) decreased, leading to improved interactive networks for efficient photo-generated exciton diffusion and transfers.^{10,11} However, nanoscale cracks and pinholes did form on the film surface during the ligand treatment process. The PC₆₀BM layer, which had an optimal thickness (here, around 20 nm) filled the nanocracks, covered the blend surface, and improved the interfacial contacts between the hybrid blend and the top electrode. An extremely thin PC₆₀BM layer could not be applied uniformly on top of the hybrid blend, and many of the nanocracks remained uncovered, exposing areas of the hybrid blend. By contrast, the relatively thick PC₆₀BM layer increased the distance through which charge carriers travel to reach the cathode, which unintentionally induced carrier recombination loss. The decrease in PCE for HSCs prepared with the thick PC₆₀BM layer is strongly associated with the low FF, as shown in Fig. 2c. The steep $J-V$ curve measured in the HSC prepared with the thick PC₆₀BM layer could be ascribed to losses by resistance, an imbalance between the electron and hole mobilities, shunt leakage paths, or etc.⁴⁴ Roughly, the electron mobility in a pure PC₆₀BM film (10^{-2} cm²/V·s)⁴⁵ is almost two order larger than hole mobilities in a PTB1 solid (4.5×10^{-4} cm²/V·s)³⁷ or an EDT-treated PbS QD solid (10^{-4} cm²/V·s).⁴⁶ Full surface coverage of the hybrid blend by a uniform PC₆₀BM layer was, therefore, crucial for enhancing the performances of the HSCs. Once this condition was met, a thinner PC₆₀BM layer was favorable for better device performances. Besides, it has been known that a fullerene interlayer can protect the photoactive layers against oxygen and humidity, thereby improving device stability.⁴⁷ Polymer:fullerene BHJs in OSCs tend to suffer from instabilities in the meta-stable film structure because fullerene tends to form aggregates at high temperatures.^{48,49} Separating PC₆₀BM from the polymer matrix may overcome photo-induced aggregation in a blend film.

Conclusions

We demonstrated the utility of a multifunctional PC₆₀BM interlayer in a polymer-QD hybrid BHJ solar cell. A thin PC₆₀BM layer deposited on top of a hybrid blend via solution processing generated excitons by harvesting photon energies at the shorter wavelengths in the solar spectrum and formed an efficient vertical D:A/A' junction at the interface with the hybrid blend. PC₆₀BM displayed strong n-type character, increased the probability of ultrafast exciton dissociation, provided intermediate pathways that improved the efficiency of photo-generated electron transport toward the top electrode, and blocked holes to reduce recombination losses. In addition to these opto-electronic benefits, an optimally thick PC₆₀BM layer covered nanoscale cracks that formed on the hybrid BHJ film surface due to QD ligand exchange with the thiol, thereby providing a uniform interfacial contact between the hybrid blend and the top electrode to reduce the contact resistance and improve the efficiency of charge extraction. These benefits significantly enhanced the PCE in the HSCs from 2.34% for the HSCs developed without a PC₆₀BM layer to 4.53% for HSCs developed with an optimally thick PC₆₀BM layer. This PCE is the highest yet reported for PbS QD-based HSCs. We believe that this study provides new routes to the fabrication of high-efficiency HSCs using simple, cost-effective, low-temperature solution processing methods. Future investigations will focus on comparing the efficiencies and long-term stabilities of HSCs developed with fullerene molecules embedded inside or outside of the hybrid photoactive films.

Experimental details

Device fabrication

PTB1 (Lumtec) and PC₆₀BM (Nano-C) were purchased and were used as received without purification. The synthesis of the colloidal PbS QDs is described elsewhere.⁹ The hybrid blend solution was prepared by dissolving PTB1 and PbS in a chloroform solvent to a total polymer-to-QD ratio of 1:9 (wt/wt), followed by magnetic stirring at 40°C overnight. The HSCs were fabricated by spin-coating PEDOT:PSS onto a glass substrate with pre-patterned ITO electrodes, followed by drying at 150°C for 10 min. A photoactive film composed of the fully mixed hybrid blend solution and with a thickness of 100 nm was spin-coated onto the PEDOT:PSS layer. Post-deposition ligand treatment was performed to exchange the pre-formed oleic acid with an end-functional group. A 100 μL volume of a 1% EDT in acetonitrile solution was casted onto the hybrid blend film and was spin-coated for 1 min. The film was washed using pure acetonitrile to remove free-standing molecules. Then, PC₆₀BM dissolved in chlorobenzene (10 mg/mL) was spin-coated on top of the ligand-exchanged hybrid blend layer. The concentration and spin speed were controlled to modulate the thickness of the PC₆₀BM layer. After EDT treatment, the hybrid blend film remained stable during the upper layer coating step. An Al electrode was thermally evaporated onto the PC₆₀BM layer through a shadow mask under high vacuum conditions with a pressure of 3×10^{-6} Torr. The complete device consisted of an ITO/PEDOT:PSS (35 nm)/hybrid nanocomposite (100 nm)/PC₆₀BM (*ca.* 10, 20, or 45 nm)/Al (100 nm).

$I-V$ measurements of the hybrid blend films

The photocurrents in the PTB1:PbS QD blends were obtained by fabricating interdigitated finger-like electrodes on a standard glass substrate via a lift-off process. A photoresist (PR, AZ 5214E, AZ Electronic Materials) was spin-coated onto the glass substrate and then exposed to UV light through a patterned photomask. After developing the exposed photoresist, a Cr/Au layer (10 nm/200 nm thick) was deposited onto the patterned PR using an electron beam evaporator. The remaining PR on the substrate was removed by immersion with agitation in AZ 400T PR stripper, leaving finger-shaped interdigitated electrodes 5 μm wide and separated by a 5 μm spacing. A 100 μL volume of a chloroform solution containing PTB1 and PbS QDs in a desired ratio was spin-coated onto the electrodes. The hybrid blends were then subjected to ligand exchange using an EDT/acetonitrile solution (1/99 vol %) for 1 min. The $I-V$ curves of the hybrid blends were obtained using an Agilent 4155C semiconductor parameter analyzer (Agilent Technologies) under UV illumination with a wavelength of 365 nm.

Characterization

The optical absorption spectra of the hybrid blends were measured using a Cary 5000 UV-vis-NIR spectrophotometer (Varian). The PL intensity spectra were measured using a focused 630 nm diode laser for excitation (10 W/cm²). The PL signal was detected using a fiber-coupled NIRQuest 512 NIR-spectrofluorometer equipped with an InGaAs array detector (Ocean Optics). The surface topographic images of the hybrid blends before and after PC₆₀BM interlayer deposition were obtained using a Xe-100 AFM (Park Systems). The samples used for cross-sectional microscopy imaging were prepared by focused ion-beam (FIB) machining using a Quanta 3D FEG (FEI) equipped with an SEM. The $J-V$ characteristics of the HSCs were measured using a source-meter (Keithley 2400) under AM 1.5G illumination with an intensity of 100 mW/cm². The solar simulator white light was provided by a 450 W Xe lamp (Oriel) equipped with an AM 1.5G filter. The EQE spectra were measured using a 300 W

Xe light source and a monochromator in a K3100 Spectral IPCE Measurement System (McScience). The photovoltaic performance measurements were performed under ambient conditions.

Acknowledgements

This research was supported by the Pioneer Research Center Program through the National Research Foundation of Korea funded by the Ministry of Science, ICT and Future Planning (NRF-2013M3C1A3065040).

Notes and references

^aNanophotonics Research Center, Korea Institute of Science and Technology, Seoul 136-791, Republic of Korea. E-mail: hikoel@kist.re.kr

^bDepartment of Molecular Science and Technology, Ajou University, Suwon 443-749, Republic of Korea.

^cDepartment of Electrical and Computer Engineering, Ajou University, Suwon 443-749, Republic of Korea

^dDepartment of Applied Chemistry, Kyung Hee University, Yongin 446-701, Republic of Korea. E-mail: dhko@khu.ac.kr

- M. Wright and A. Uddin, *Sol. Energy Mater. Sol. Cells*, 2012, **107**, 87.
- W. U. Huynh, J. J. Dittmer and A. P. Alivisatos, *Science*, 2002, **295**, 2425.
- A. P. Alivisatos, *Science*, 1996, **271**, 933.
- O. E. Semonin, J. M. Luther, S. Choi, H.-Y. Chen, J. Gao, A. J. Nozik and M. C. Beard, *Science*, 2011, **334**, 1530.
- D. Wang, J. K. Baral, H. Zhao, B. A. Gonfa, V. Truong, M. A. E. Khakani, R. Izquierdo and D. Ma, *Adv. Funct. Mater.*, 2011, **21**, 4010.
- H. C. Leventis, S. P. King, A. Sudlow, M. S. Hill, K. C. Molloy and S. A. Haque, *Nano Lett.*, 2010, **10**, 1253.
- Y. Zhou, M. Eck, C. Veit, B. Zimmermann, F. Rauscher, P. Niyamakom, S. Yilmaz, I. Dumsch, S. Allard, U. Scherf and M. Krüger, *Sol. Energy Mater. Sol. Cells*, 2011, **95**, 1232.
- W. U. Huynh, J. J. Dittmer, W. C. Libby, G. L. Whiting and A. P. Alivisatos, *Adv. Funct. Mater.*, 2003, **13**, 73.
- D. Celik, M. Krueger, C. Veit, H. F. Schleiermacher, B. Zimmermann, S. Allard, I. Dumsch, U. Scherf, F. Rauscher and P. Niyamakom, *Sol. Energy Mater. Sol. Cells*, 2012, **98**, 433.
- S. Ren, L.-Y. Chang, S.-K. Lim, J. Zhao, M. Smith, N. Zhao, V. Bulović, M. Bawendi and S. Gradedčak, *Nano Lett.*, 2011, **11**, 3998.
- R. Zhou, R. Stalder, D. Xie, W. Cao, Y. Zheng, Y. Yang, M. Plaisant, P. H. Holloway, K. S. Schanze, J. R. Reynolds and J. Xue, *ACS Nano*, 2013, **7**, 4846.
- J. Seo, W. J. Kim, S. J. Kim, K.-S. Lee, A. N. Cartwright and P. N. Prasad, *Appl. Phys. Lett.*, 2009, **94**, 133302.
- M. Nam, J. Park, S.-W. Kim and K.-K. Lee, *J. Mater. Chem. A*, 2014, **2**, 3978.
- M. Nam, S. Kim, S. Kim, S.-W. Kim and K.-K. Lee, *Nanoscale*, 2013, **5**, 8202.
- J. J. Choi, Y.-F. Lim, M. B. Santiago-Berrios, M. Oh, B.-R. Hyun, L. Sun, A. C. Bartnik, A. Goedhart, G. G. Malliaras, H. D. Abruña, F. W. Wise and T. Hanrath, *Nano Lett.*, 2009, **9**, 3749.
- J. Seo, M. J. Cho, D. Lee, A. N. Cartwright and P. N. Prasad, *Adv. Mater.*, 2011, **23**, 3984.
- Z. Liu, Y. Sun, J. Yuan, H. Wei, X. Huang, L. Han, W. Wang, H. Wang and W. Ma, *Adv. Mater.*, 2013, **25**, 5772.
- Z. He, C. Zhong, S. Su, M. Xu, H. Wu and Y. Cao, *Nat. Photon.*, 2012, **6**, 591.
- G. Dennler, M. C. Scharber and C. J. Brabec, *Adv. Mater.*, 2009, **21**, 1323.
- H. Nagaoka, A. E. Colbert, E. Strein, E. M. Janke, M. Salvador, C. W. Schlenker and D. S. Ginger, *J. Phys. Chem. C*, 2014, **118**, 5710.
- O. Voznyy, D. Zhitomirsky, P. Stadler, Z. Ning, S. Hoogland and E. H. Sargent, *ACS Nano*, 2012, **6**, 8448.
- K. M. Noone, E. Strein, N. C. Anderson, P.-T. Wu, S. A. Henekhe and D. S. Ginger, *Nano Lett.*, 2010, **10**, 2635.
- Y. Zhang, Z. Li, J. Ouyang, S.-W. Tsang, J. Lu, K. Yu, J. Ding and Y. Tao, *Org. Electron.*, 2012, **13**, 2773.
- C. M. Chuang, P. R. Brown, V. Bulović and M. G. Bawendi, *Nat. Mater.*, 2014, **13**, 796.
- M. Yuan, O. Voznyy, D. Zhitomirsky, P. Kanjanaboos and E. H. Sargent, *Adv. Mater.*, 2015, **27**, 917.
- P. Wang, A. Abrusci, H. M. P. Wong, M. Svensson, M. R. Andersson and N. C. Greenham, *Nano Lett.*, 2006, **6**, 1789.
- M. D. Heinemann, K. von Maydell, F. Zutz, J. Kolny-Olesiak, H. Borchert, I. Riedel and J. Parisi, *Adv. Funct. Mater.*, 2009, **19**, 3788.
- L. Zhao, X. Pang, R. Adhikary, J. W. Petrich and Z. Lin, *Angew. Chem. Int. Ed.*, 2011, **50**, 3958.
- L. Zhao, X. Pang, R. Adhikary, J. W. Petrich, M. Jeffries-EL and Z. Lin, *Adv. Mater.*, 2011, **23**, 2844.
- G. Itskos, P. Papagiorgis, D. Tsokkou, A. Othonos, F. Hermerschmidt, S. P. Economopoulos, M. Yarema, W. Heiss and S. Choulis, *Adv. Energy Mater.*, 2013, **3**, 1490.
- J. Jung, X. Pang, C. Feng and Z. Lin, *Langmuir*, 2013, **29**, 8036.
- W. Fu, L. Wang, J. Ling, H. Li, M. Shi, J. Xue and H. Chen, *Nanoscale*, 2014, **6**, 10545.
- D. Jarzab, K. Szendrei, M. Yarema, S. Pichler, W. Heiss and M. A. Loi, *Adv. Funct. Mater.*, 2011, **21**, 1988.
- B.-R. Hyun, Y.-W. Zhong, A. C. Bartnik, L. Sun, H. D. Abruña, F. W. Wise, J. D. Goodreau, J. R. Matthews, T. M. Leslie and N. F. Borrelli, *ACS Nano*, 2008, **2**, 2206-2212.
- W.-K. Koh, S. R. Saudari, A. R. Fafarman, C. R. Kagan and C. B. Murray, *Nano Lett.*, 2011, **11**, 4764.
- H.-Y. Chen, J. Hou, S. Dayal, L. Huo, N. Kopidakis, M. C. Beard and J. M. Luther, *Adv. Energy Mater.*, 2011, **1**, 528.
- Y. Liang, Y. Wu, D. Feng, S.-T. Tsai, H.-J. Son, G. Li and L. Yu, *J. Am. Chem. Soc.*, 2009, **131**, 56.
- S.-W. Tsang, H. Fu, J. Ouyang, Y. Zhang, K. Yu, J. Lu and Y. Tao, *Appl. Phys. Lett.*, 2010, **96**, 243104.

Journal Name

39. N. Zhao, T. P. Osedach, L.-Y. Chang, S. M. Geyer, D. Wanger, M. T. Binda, A. C. Arango, M. G. Bawendi and V. Bulovic, *ACS Nano*, 2010, **4**, 3743.
40. Y. Chiba, A. Islam, Y. Watanabe, R. Komiya, N. Koide and L. Han, *Jpn. J. Appl. Phys.*, 2006, **45**, L638.
41. S. J. Yoon, J. H. Park, H. K. Lee and O. O. Park, *Appl. Phys. Lett.*, 2008, **92**, 143504.
42. B. R. Saunders and M. L. Turner, *Adv. Colloid Interf. Sci.*, 2008, **138**, 1.
43. C. J. Brabec, S. E. Shaheen, C. Winder, N. S. Sariciftci and P. Denk, *Appl. Phys. Lett.*, 2002, **80**, 1288.
44. Z. Liu and E.-C. Lee, *J. Appl. Phys.*, 2012, **11**, 023104.
45. E. von Hauff, V. Dyakonov and J. Parisi, *Sol. Energy Mater. Sol. Cells*, 2005, **87**, 149.
46. E. J. D. Klem, H. Shukla, S. Hinds, D. D. MacNeil, L. Levina and E. H. Sargent, *Appl. Phys. Lett.*, 2008, **92**, 212105.
47. T. Shiga, K. Takechi and T. Motohiro, *Sol. Energy Mater. Sol. Cells*, 2006, **90**, 1849.
48. M. Jørgensen, K. Norrman, S. A. Gevorgyan, T. Tromholt, B. Andreasen and F. C. Krebs, *Adv. Mater.*, 2012, **24**, 580.
49. X. Yang, J. K. J. van Duren, R. A. J. Janssen, M. A. J. Michels and J. Loos, *Macromolecules*, 2004, **37**, 2151.

We describe a new platform for developing high-efficiency polymer-colloidal quantum dot hybrid solar cells employing a multifunctional fullerene interlayer.

